IMECE2019-11908

CONCURRENT-FLOW FLAME SPREAD OVER A THIN SOLID IN A NARROW CONFINED SPACE IN MICROGRAVITY

Yanjun Li¹, Ya-Ting T. Liao¹, Paul Ferkul²

¹Case Western Reserve University, Cleveland, OH ²Universities Space Research Association, Cleveland, OH

ABSTRACT

A numerical study is pursued to investigate the aerodynamics and thermal interactions between a spreading flame and the surrounding walls as well as their effects on fire behaviors. This is done in support of upcoming microgravity experiments aboard the International Space Station. For the numerical study, a three-dimensional transient Computational Fluid Dynamics combustion model is used to simulate concurrent-flow flame spread over a thin solid sample in a narrow flow duct. The height of the flow duct is the main parameter. The numerical results predict a quenching height for the flow duct below which the flame fails to spread. For duct heights sufficiently larger than the quenching height, the flame reaches a steady spreading state before the sample is fully consumed. The flame spread rate and the pyrolysis length at steady state first increase and then decrease when the flow duct height decreases. The detailed gas and solid profiles show that flow confinement has competing effects on the flame spread process. On one hand, it accelerates flow during thermal expansion from combustion, intensifying the flame. On the other hand, increasing flow confinement reduces the oxygen supply to the flame and increases conductive heat loss to the walls, both of which weaken the flame. These competing effects result in the aforementioned non-monotonic trend of flame spread rate as duct height varies. This work relates to upcoming microgravity experiments, in which flat thin samples will be burned in a lowspeed concurrent flow using a small flow duct aboard the International Space Station. Two baffles will be installed parallel to the fuel sample (one on each side of the sample) to create an effective reduction in the height of the flow duct. The concept and setup of the experiments are presented in this work.

Keywords: tunnel height effect, microgravity combustion, concurrent flame spread, near quenching oscillation

1. INTRODUCTION

Fires in confined spaces (e.g., cavity walls in buildings, transportation vehicles, tunnels) are a major safety concern. They result in significant numbers of injuries, deaths, and

property losses every year [1]. In confined spaces, fire behaviors can be very different from fires in open spaces. To address this concern, many past studies have focused on the mechanical (or aerodynamic) interactions between structures and fires, using stationary burners in rooms, corners, tunnels, between parallel panels, or near walls [2, 3, 4, 5, 6]. Other studies have focused on tunnel fires with ventilated flows [7, 8, 9, 10, 11, 12, 13, 14]. In most of these studies, fires are simulated experimentally using stationary burners – the flame does not move. However, in most situations, real fires in confined spaces involve flames that themselves move or spread across the fuel.

Flame spread is one of the most important characteristics of a fire, as it determines the available time to control the fire or to escape the area. There have been extensive efforts studying flame spread over solid materials using microgravity experiments. In microgravity, buoyancy is essentially eliminated and hence forced flow can be imposed on the sample independent of other parameters. For concurrent-flow flame spread in microgravity, limiting flame lengths and steady spread rates were predicted by numerical models [15, 16]. They were also verified in space experiments aboard the International Space Station (ISS) where thick plastic rods [17] and thin fabric samples [18] were burned in low-speed concurrent flows in a small duct (duct height ~10 cm).

In a recent NASA project, a series of large-scale flame spread experiments were conducted in unmanned space vehicles [19]. The dimensions of the sample and the flow duct used in these experiments were significantly larger (duct height $\sim 40~\rm cm)$ than prior experiments. Results yielded significantly smaller flame spread rates than seen in previous smaller-scale experiments for the same thin fabric, even though all other environmental conditions were the same (oxygen, pressure, and flow speed). This observation that flames spread faster in smaller ducts is suspected to be due to thermal expansion during combustion which causes acceleration because the flow is more confined. This is referred to as the chimney effect. The increased radiation heat feedback from duct walls to the flame and to the fuel surface may also be a factor.

Several research groups have numerical studies that address this situation. For instance, an earlier simulation using a steady two-dimensional model (capable of only finding steady-state solutions) by Shih and T'ien showed that the concurrent flame spread rate increases as the tunnel height decreases [20]. consistent with the experimentally observed phenomena. However, in their simulation, Shih and T'ien showed that when the tunnel height is very small, conductive heat loss to the tunnel walls increases, slowing the spread rate. This eventually leads to flame quenching. Their results also show that for the same tunnel height, the flame becomes longer and the spread rate increases when the reflectivity of the tunnel wall increases. No steady state solution was achieved for wall reflectivity of ~1. It is suspected that the flame continuously grows while traveling downstream (a transient process) and hence cannot be captured by a steady model. Even if the flame eventually reaches a steady state, the computational domain is unable to capture such a hypothetically large flame.

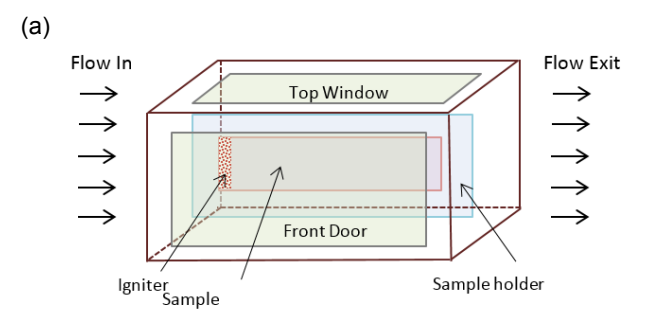
The objective of this work is to attain a complete understanding of the effects of the confinement on flame spread over solid combustibles and to explore the fate (steady, growing, or quenched) of flames in different confinement conditions. This will be achieved through a series of microgravity experiments conducted aboard the ISS. In the meantime, we conduct numerical simulation using a custom in-house Computational Fluid Dynamics (CFD) model. In this paper, we will introduce the concept of the experiments and present the results of our numerical simulation.

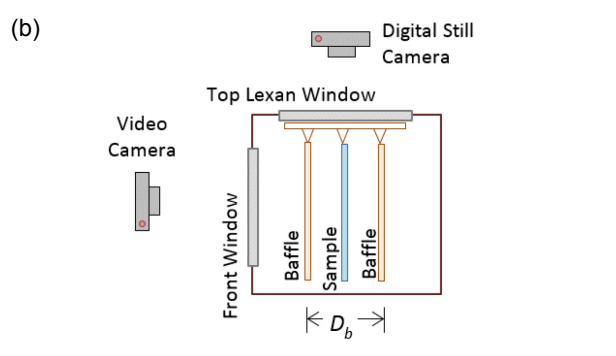
2. MICROGRAVITY EXPERIMENT

The setup of the microgravity experiment is shown in Fig. 1. It leverages the existing BASS (Burning and Suppression of Solids) wind tunnel facility situated in the Microgravity Science Glovebox (MSG) aboard the ISS [21, 17, 18, 22]. The wind tunnel has a cross-sectional area of 7.6 cm × 7.6 cm and a length of 20 cm (see Fig. 1a). Samples (2.2 cm wide, 10 cm long) will be mounted on a stainless steel sample holder in the flow duct and will be ignited by a hot wire at the upstream leading edge (see Fig. 1c).

In this work, we will create an effective reduction in the height of the tunnel by adding two baffles parallel and adjacent to the fuel sample, one on each side of the sample (see Fig. 1b). The baffles will be mounted on an adjustable rack so that the distance between the baffles (D_b) can be changed in 1-cm increments between 1.0 and 5.0 cm. This will allow us to explore the limiting quenching distance and to precisely determine the regimes of steady and growing flames (if they exist). We also use baffles with different surface treatments, simulating different radiative wall properties. Examples include transparent polycarbonate, blackened aluminum (reflectivity~0), and polished metal (reflectivity~1). This allows us to investigate the radiative interactions between the tunnel wall and the spreading flame. Two sample materials will be tested: 1mm-thick PMMA slabs and a cotton-blend fabric (75% cotton and 25% fiberglass). called SIBAL. The igniter will be integrated into each sample for one-time use. The testing conditions will be 21% oxygen at 1

atm. The flow speeds of interest are 2 to 5 cm/s. The main source of data will be derived from digital images of the flame from which we can measure flame size, growth, spread rate, and quenching. The microgravity experiments are scheduled to begin in late 2019.





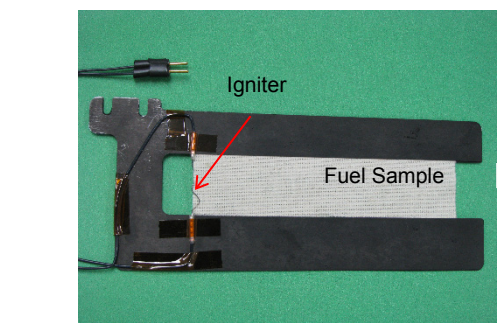


Figure 1: Experimental setup (not to scale). (a) Three-dimensional schematics of the modified BASS wind tunnel (baffles are not shown) (b) Schematics of the edge view from the tunnel exit. (c) Fuel sample, sample holder, and igniter.

3. NUMERICAL MODEL

The numerical model used in this work is based on a previously developed three-dimensional transient CFD model. The detailed information and formulation can be found in previous papers [23, 24, 25].

The configuration of the model is based on the flow duct and sample setup in the microgravity experiments (see Fig. 2 and Table 1). The height of the flow duct (h) is the parameter in this study. It varies between 0.5 and 7.6 cm. The fuel sample, SIBAL is sandwiched by a sample holder and is placed at the center of the flow duct. Air flow at 10 cm/s is imposed at the duct inlet. Ignition is achieved by applying external heat flux at the

(c)

upstream leading edge of the sample. After ignition, the external heat flux is gradually turned off in 3 seconds. To allow sufficient time for flame development, the sample length is set to 30 cm (instead of 10 cm in the experiments) in the simulations. This facilitates observation of the eventual fate of the flame (continuously growing, steady flame spread, or extinction). The ambient conditions are at zero gravity with air temperature of 300 K and pressure of 1 atm.

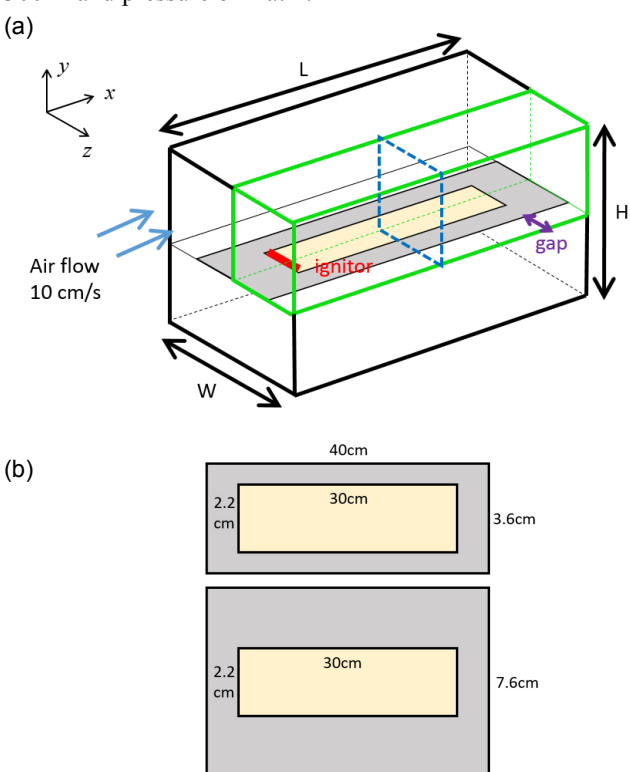


Figure 2: Model configuration (a) Sample, sample holder, and the flow duct. (b) Sample and sample holder (not to scale).

Table 1: Dimensions of sample and flow duct (unit: cm)

Tunnel size (W×L×H)	Sample holder size (W×L)	Sample size (W×L)	Sample distance to tunnel entrance	Sample distance to tunnel exit
7.6×40×h*	3.6×40 (with side gaps) 7.6×40 (no gap)	2.2×30	5	5

 $^*h = 0.5 - 7.6$ (cm).

In the simulation, constant temperature at 300K is assumed on all duct walls. Symmetry is assumed on the plane along the centerline of the fuel sample and on the plane of the sample half-thickness. This reduces the computational domain to a quarter of the flow duct (marked by the green lines in Fig. 2). The model employs a non-uniform grid structure and an automatic Adaptive Mesh Refinement (AMR) scheme. The program traces the flame location and allocates fine meshes (one-tenth of the characteristic length for thermal diffusion) in the regions near the

flame base and pyrolysis front while the flame spreads downstream. Here (and throughout the rest of this article), 'base' and 'front' refer to the most upstream and downstream points respectively of the burning region.

In the simulations, two sample holders with different widths (W) are considered. One sample holder has the same width (7.6 cm) as the flow duct. Another sample holder is narrower than the flow duct, leaving 2cm gaps between the edges of the sample holder and the duct side walls (see Fig. 2a). The sample setup has an effect on the flow profile when the flow duct height is on the order of the flow boundary layer thickness. Figure 3 shows the flow profiles on the mid cross-section of the flow duct (the plane marked by the blue dashed line in Fig. 2a) for the two sample setups (with and without the side gaps respectively) at two duct heights (h = 76mm and h = 20 mm). For the sample setup without the side gaps, it is clear that the boundary layer grows on the walls of the flow duct as well as on the surface of the sample holder. The effective area for the flow passage is reduced, resulting in flow speeds higher than the inlet velocity (10 cm/s) in the area between the sample holder and the ceiling of the flow duct. The maximum flow velocity increases when the height of the flow duct decreases.

For the sample setup with the side gaps, flow on the two sides experiences less resistance compared to the flow near the sample surface. When the flow duct height is at 20 mm (upper right plot in Fig. 3), boundary layers of the duct ceiling and of the sample surface meet. The flow is 'locked' by the viscous boundary layer in the area between the sample and the flow duct ceiling. The side gaps ventilate most of the flow. In other words, the flow that the fuel sample encounters is significantly lower than the airflow imposed at the duct inlet. This has a significant impact on the flame spread process and will be discussed further below.

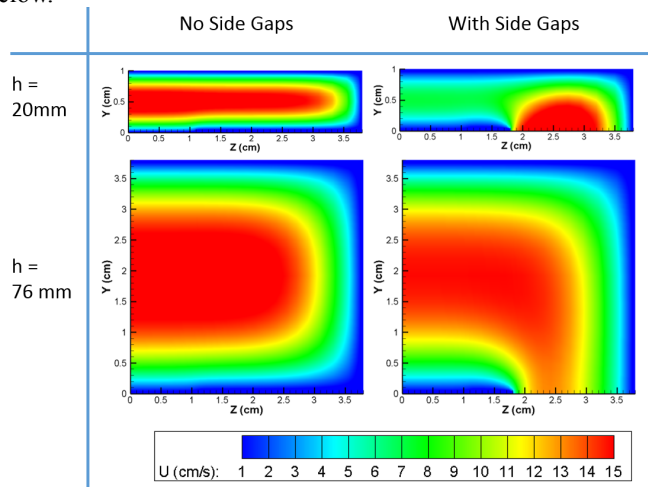


Figure 3: Flow velocity profile on the mid cross-section of the flow duct (20 cm from the upstream leading edge of the sample holder, as marked by the blue dashed line in Fig. 2a). Flow velocity at the flow duct inlet: 10 cm/s. Results are from pure flow simulation without combustion. The y-axis "Height" is the distance from the sample surface.

4. NUMERICAL RESULTS

In most of the simulated cases, steady spread was observed. Figure 4 shows the advancement of the sample burning region for h=20 mm. The burning region is defined as solid pyrolysis reaction rate $>10^{-5}$ g/cm²/s. Results of both sample setups (with and without the side gaps) show that after an initial transient period, the flame reaches a limiting length and the spread rate (slope of the pyrolysis base/front advancement) remains roughly constant. In this work, the steady spread rate is defined as the average spread rates of the pyrolysis front and base between 5 cm and 25 cm (see linear trend lines in Fig. 4). Average pyrolysis length is also calculated at the same time duration.

For the sample setup with the side gaps, the flame is shorter and spreads slower compared to the setup without the side gaps. This is because the flame encounters a smaller flow when side gaps present as explained above.

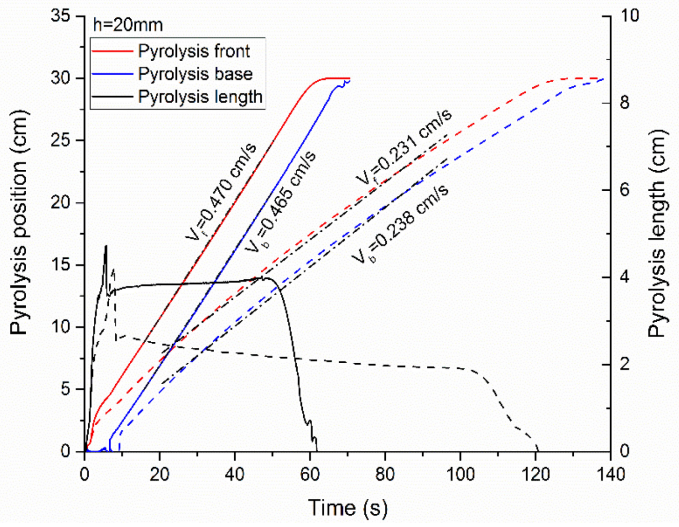


Figure 4: Location of downstream pyrolysis front, upstream pyrolysis base, and pyrolysis length versus time for h = 20 mm. Dashed lines are for sample setup with side gaps. Solid thick lines are for sample setup without side gaps.

4.1 Effect of the height of the flow duct

The steady-state pyrolysis lengths and spread rates are plotted against flow duct height in Figs. 5 and 6 respectively. For both sample setups, the pyrolysis length and spread rate first increase and then decrease when the flow duct height is reduced. Among the simulated cases, the optimal flow duct height for the flame spread occurs at 30 to 40 mm. When the flow duct height is below a critical value (~ 5 to 8 mm), the flame fails to spread to the end of the sample.

To understand this non-monotonic trend, solid and gas profiles are examined in detail. Figures 7-10 compare the oxygen profiles on the center symmetry plane and the heat flux distributions on the sample surface and duct ceiling. For these profiles, the two sample setups have similar results and hence only results for the sample setup with side gaps are shown here. Figure 7 shows that when the duct height is sufficiently large (e.g., h = 40 mm), oxygen is transported (via convection and

diffusion) to the downstream end of the duct. As the duct height is reduced, the mass flow rate of the air (and the oxygen) is expected to decrease since a constant air velocity is imposed at the duct inlet in call cases. Figure 7 shows that for $h=20 \, \mathrm{mm}$, the flame extends to the duct ceiling and consumes all the oxygen. This implies that the oxygen supply becomes a limiting factor for the combustion. The reduced oxygen supply to the flame and to the downstream region may contribute to the shorter pyrolysis length and the smaller spread rate for $h=20 \, \mathrm{mm}$ compared to $h=40 \, \mathrm{mm}$.

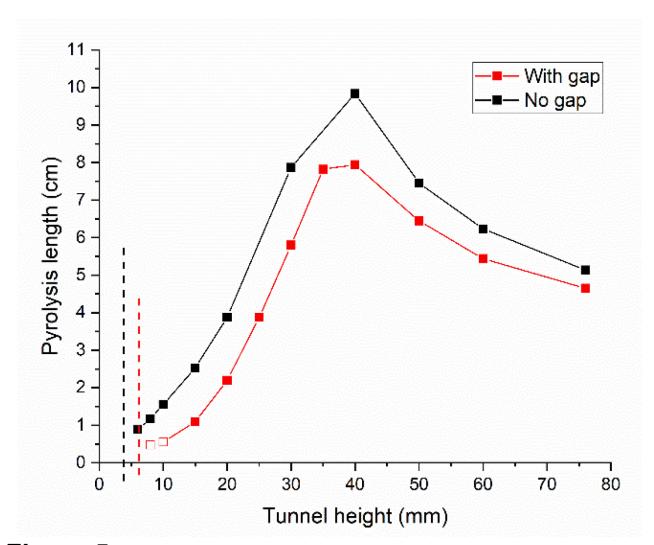


Figure 5: Pyrolysis lengths versus flow duct heights. The dashed lines denote the quench limits. Hollow symbols denote partial propagation.

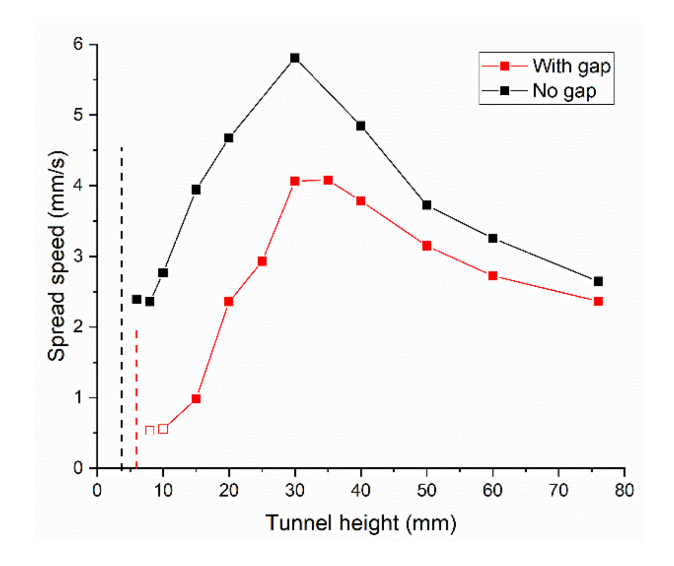


Figure 6: Flame spread rates versus flow duct heights. The dashed lines denote the quench limits. Hollow symbols denote partial propagation.

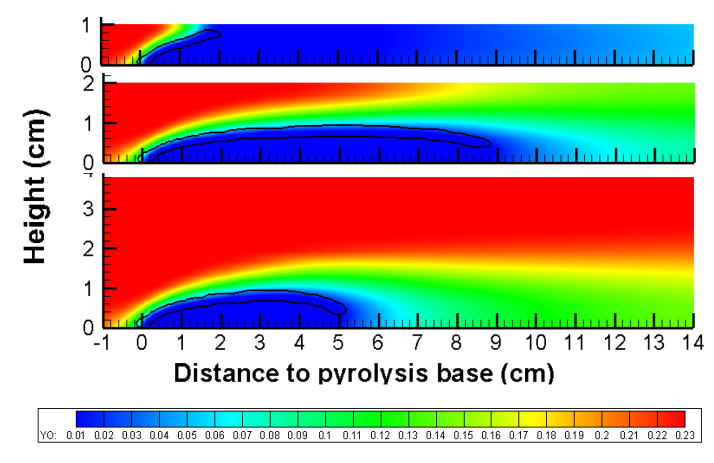


Figure 7: Mass fraction of oxygen (color contours) and flame shape (black contour) on the center symmetry plane. From to top to bottom: h = 20 mm, h = 40 mm, h = 76 mm. Flame shape is defined as the gas phase reaction at $10^{-4} \text{g/cm}^3/\text{s}$.

Figures 8 and 9 show the conductive and radiative heat fluxes on the sample surface and the duct ceiling for h = 20 mm and 76 mm. Figure 10 further compares the heat fluxes along the centerline of the sample for three different duct heights. The heat fluxes for h = 40 mm and h = 76 mm are of similar magnitudes. Conductive heat to the ceiling is negligible as the flame is far away from the ceiling. The heat loss to the ceiling is mainly due to flame radiation (hence the curves coincide with the net heat flux onto the duct ceiling for h=40 and 76 mm in Fig. 10). At h=20 mm, the flame is in close proximity to the duct ceiling (see Fig. 7). Thus, the conductive heat loss to the ceiling becomes much larger and is comparable to the conductive heat feedback to the sample surface. Also note that at h=20 mm, the radiation heat loss to the ceiling is approximately twice of that at h=40 mm and 76 mm.

For heat fluxes on the sample surface, Figs. 8 and 10 show that the conductive heat flux from the flame to the sample surface decreases as the height of the flow duct increases. This is reasonable as the confinement imposed by the duct ceiling forces the flame to stay close to the sample surface, enhancing the conductive and net heat fluxes near the upstream flame base region. In other word, a higher local burning rate (or fuel mass flux on the sample) near the flame base is expected for a smaller duct height, despite the fact that the pyrolysis length might be smaller due to the oxygen limitation as explained above.

The flow velocity profiles at different flow duct heights are also compared. Figures 11 shows profiles at the center symmetry plane for $h=20\,$ mm, 40 mm, and 76 mm. Note that for $h=40\,$ mm and 76 mm, flow profiles on the center plane using the two different sample setups are similar and hence only one result is shown. It is evident that in these cases (large duct heights), the flow accelerates due to the thermal expansion during the combustion process. This effect becomes more and more significant when the duct height decreases. Compared to $h=76\,$ mm, the flow for $h=40\,$ mm is stronger, and as a consequence, the flame is longer.

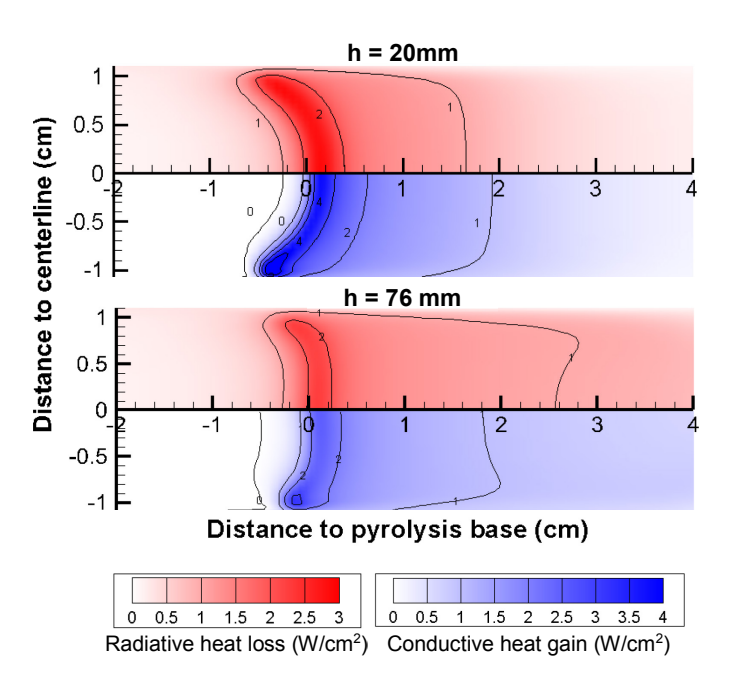


Figure 8: Distributions of the conductive heat gain (blue contours on the bottom plots) and radiative heat loss (red contours on the top plots) on the sample surface at h = 20 mm and h = 76 mm.

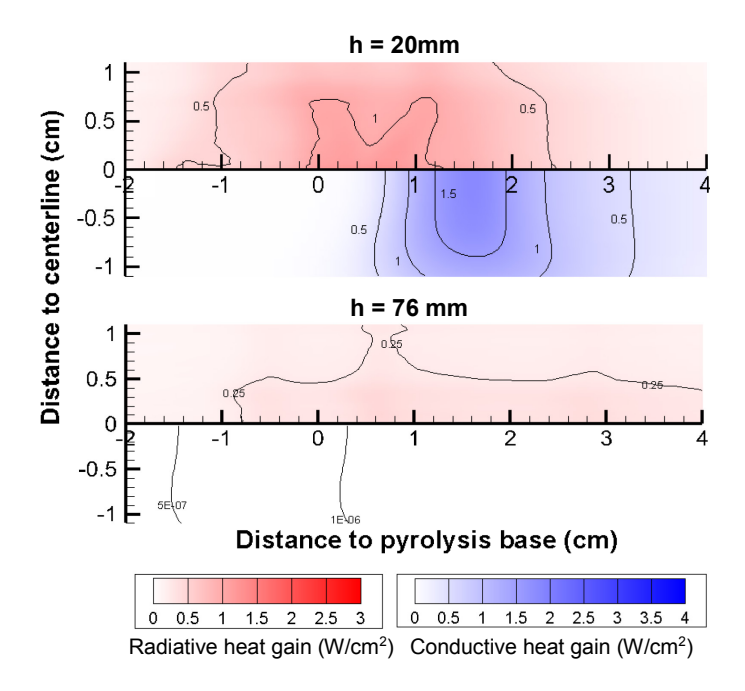


Figure 9: Distribution of the conductive (blue contours on the bottom plots) and radiative heat flux (red contours on the top plots) into the duct ceiling at h = 20 mm and h = 76 mm.

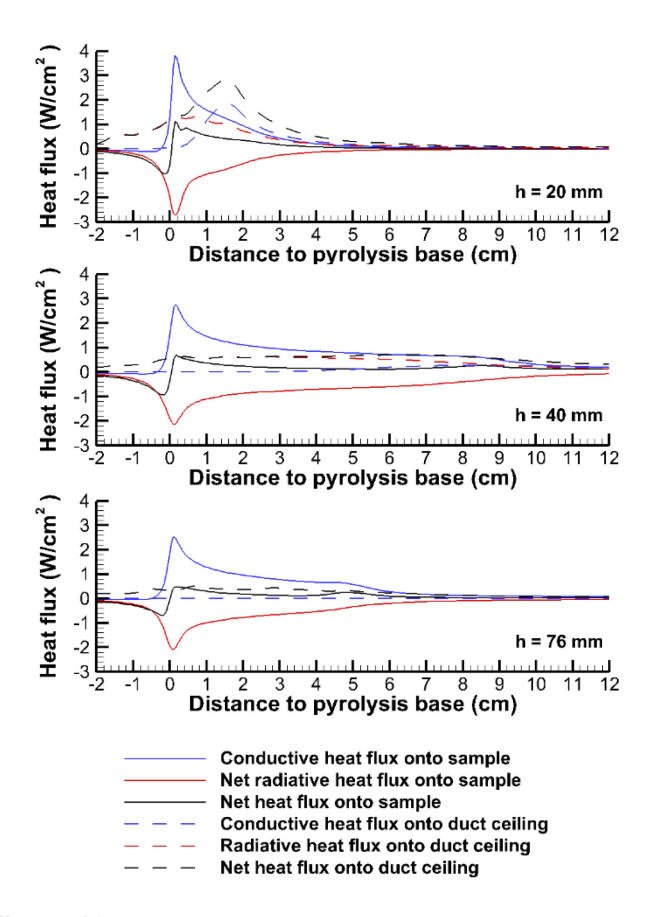


Figure 10: Conductive and radiative heat fluxes along the sample centerline. From top to bottom: h = 20 mm, h = 40 mm, and 76mm.

For small duct heights (e.g., h = 20 mm in Fig. 11), simulations with sample setup with and without side gaps show different results. For sample setups without the side gaps, the flow accelerates due to the thermal expansion as discussed above. However, when side gap presents, the flow is diverted to the side gaps. The flow speed on the center symmetry plane is low even after thermal expansion. This effect, in addition to the reduced oxygen supply and the increased heat loss to the ceiling, contributes to the decreased spread rate and pyrolysis length when duct height decreases. Note that both the quenching height and the optimal duct height for flame spread are slightly higher for sample setups with side gaps compared to those without gaps.

4.2 Near limit oscillation

As mentioned above, there exists a quenching duct height below which no flame spread is observed. Near this limit, the pyrolysis length was observed to oscillate for sample setups with gaps (Fig. 12). The maximum gas temperature and its location relative to the upstream pyrolysis base also exhibit in-phase oscillations (Fig. 13). This phenomenon was reported in previous works for candle flames [26], edge flames [27], pool fires [28], opposed-flow diffusion flames [29, 30] and concurrent-flow diffusion flames [31]. It was attributed to thermo-diffusive instability.

The flame and solid profiles in one cycle (~2s) are examined in Fig. 14. The solid mass loss rate (see black lines in Fig. 14 bottom plots) indicates that the flame splits and merges in the lateral (cross-stream) direction. In the first half of the cycle, two flamelets near the sample sides grow laterally and merge at the center. In the second half of the cycle, the flame splits laterally and forms two flamelets. Then, the next period starts. This interesting phenomenon warrants further investigations in future work.

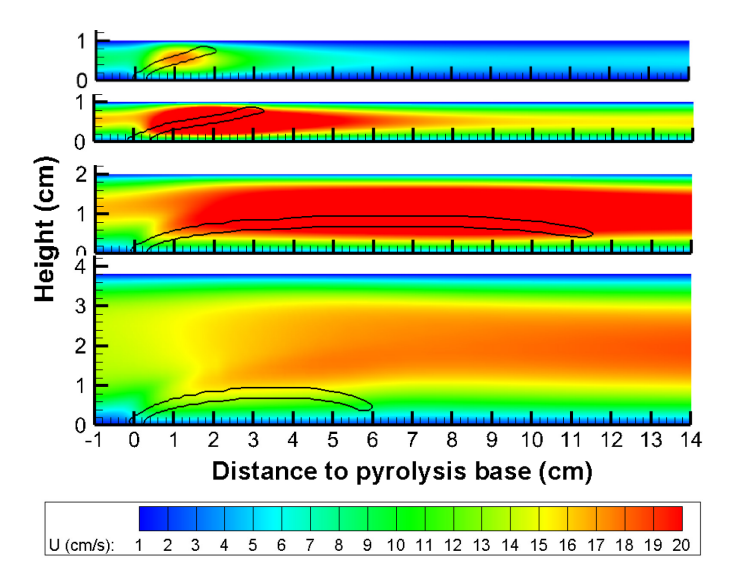


Figure 11: Stream-wise flow velocity (color contours) and flame shape (black contour) on the center symmetry plane. From top to bottom: h = 20 mm, h = 20 mm, h = 40 mm, h = 76 mm. Sample holder width: 36mm (with side gaps) in the top first plot. 76 mm (no side gaps) in the bottom three plots. Flame shape is defined as the gas phase reaction at $10^{-4}\text{g/cm}^3/\text{s}$.

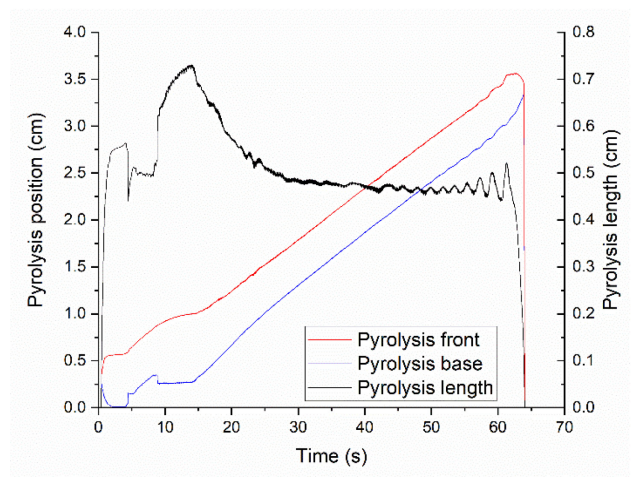


Figure 12: Near quenching oscillation: Location of pyrolysis front, pyrolysis base, and pyrolysis length on the center symmetry plane (h = 8 mm for sample setup with side gaps).

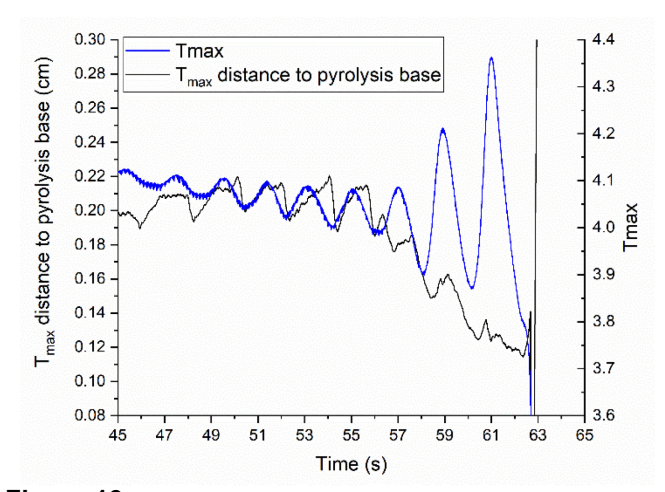


Figure 13: Near quenching oscillation: Maximum gas temperature and its position relative to the upstream pyrolysis base (h = 8 mm with sample setup with side gaps).

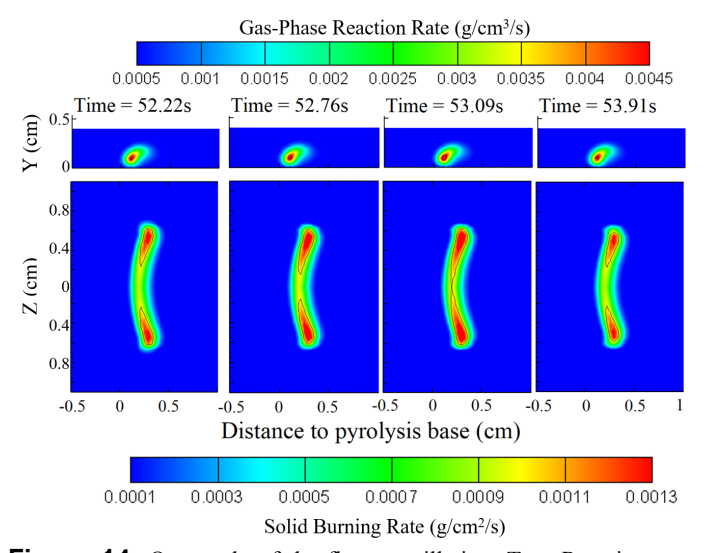


Figure 14: One cycle of the flame oscillation. Top: Reaction rate contour on the center symmetry plane. The solid line denotes reaction rate at $0.0045 \, \text{g/cm}^3/\text{s}$. Bottom: Mass loss rate on solid surface. The solid line denotes mass loss rate at $0.001 \, \text{g/cm}^2/\text{s}$

5. CONCLUSION

A three-dimensional transient CFD code was used to simulate concurrent-flow flame spread over thin solid materials in a low-speed flow duct. The height of the flow duct is varied to study the effect of confinement and the flame-wall aerodynamics/thermal interactions. The main findings from the simulation results are:

- 1) In most simulated cases, the flame reaches a steady spreading state before the sample is consumed. The flame spread rate and the pyrolysis length at steady state first increase then decrease when the flow duct height decreases.
- 2) The flow confinement imposed by the duct has multiple effects on the flame spreading process. On one hand, it accelerates the flow when the flow experiences thermal expansion during combustion. The confinement also forces the

flame to stay close to the sample surface, enhancing the net heat flux and local solid burning rate near the upstream flame base. These effects intensify the flame. On the other hand, it limits the oxygen supply to the flame in the downstream region. The flame also loses heat to the duct walls through conduction and radiation, reducing the strength of the flame. These competing effects results in the above-mentioned non-monotonic trend of the flame spread rate and pyrolysis length at different duct heights.

- 3) When the duct height is on the order of the thickness of the flow viscous boundary layer, the setup of the sample plays a significant role on the experiment. In our cases, a flat thin sample is placed in the center of the flow duct and it (or its holder) does not span across the width of the duct, leaving gaps on the two sides. Flow is diverted to the side gaps and the actual flow speed in the sample region is significantly lower than the flow imposed at the duct inlet. This reduces the flammability of the sample.
- 4) When the height of the duct is below a critical quenching height, no flame spread is observed. Near this limit, oscillation of the pyrolysis length is observed. The flame splits and merges periodically in the lateral direction before the flame dies. This phenomenon is suspected to be due to the thermo-diffusive instability and will be investigated further in future work.

The numerical experiments are done in support of upcoming microgravity experiments aboard the ISS. Tests of concurrent-flow flame spread over flat samples will be conducted in an existing flow duct (BASS facility). A wide range of parameters will be tested, including duct height, sample material, duct wall surface properties, flow speed, and oxygen concentration.

ACKNOWLEDGEMENTS

This work is supported by National Science Foundation under grant number CBET-1740478. The authors would also like to thank CASIS (Center for the Advancement of Science in Space) and ZIN Technologies for the technical support on the microgravity experiments. This work made use of the High Performance Computing Resource in the Core Facility for Advanced Research Computing at Case Western Reserve University.

REFERENCES

- [1] H. J. G. Haynes, "Fire Loss in the United States During 2015," National Fire Protection Association, 2016.
- [2] B. Y. Lattimer and U. Sorathia, "Thermal Characteristics of Fires in a Noncombustible Corner," *Fire Safety Journal*, vol. 38, pp. 709-745, 2003.
- [3] B. Y. Lattimer and U. Sorathia, "Thermal Characteristics of Fires in a Combustible Corner," *Fire Safety Journal*, vol. 38, pp. 747-770, 2003.
- [4] M. Poreh and G. Garrad, "A Study of Wall and Corner Fire Plumes," *Fire Safety Journal*, vol. 34, pp. 81-98, 2000.
- [5] O. Megret and O. Vauquelin, "A Model to Evaluate Tunnel Fire Characteristics," *Fire Safety Journal*, vol. 34, pp. 393-401, 2000.

- [6] D. A. B. Kristin L.T. Jamison, "A new fire performance test for cavity wall insulation," MATEC Web of Conferences, p. 02004, 2016.
- [7] L. H. Hu, R. Huo, H. B. Wang, Y. Z. Li and R. X. Yang, "Experimental Studies on Fire-Induced Buoyant Smoke Temperature Distribution along Tunnel Ceiling," *Building and Environment*, vol. 42, pp. 3905-3915, 2007.
- [8] L. H. Hu, W. Peng and R. Huo, "Critical Wind Velocity for Arresting Upwind Gas and Smoke Dispersion Induced by Near-Wall Fire in a Road Tunnel," *Journal of Hazardous Materials*, vol. 150, pp. 68-75, 2008.
- [9] J. S. Roh, S. S. Yang, H. S. Ryou, M. O. Yoon and Y. T. Jeong, "An Experimental Study on the Effect of Ventilation Velocity on Burning Rate in Tunnel Fires Heptane Pool Fire Case," *Building and Environment*, vol. 43, pp. 1225-1231, 2008.
- [10] H. Ingason and Y. Z. Li, "Model Scale Tunnel Fire Tests with Longitudinal Ventilation," *Fire Safety Journal*, vol. 45, pp. 371-384, 2010.
- [11] J. P. Kunsch, "Simple Model for Control of Fire Gases in a Ventilated Tunnel," *Fire Safety Journal*, vol. 37, pp. 67-81, 2002.
- [12] M. Weng, X. Lu, F. Liu and C. Du, "Study on the critical velocity in a sloping tunnel fire under longitudinal ventilation," *Applied Thermal Engineering*, vol. 94, pp. 422-434, 2016.
- [13] F. Tang, L. Li, M. Dong, Q. Wang, F. Mei and L. Hu., "Characterization of buoyant flow stratification behaviors by Richardson(Froude) number in a tunnel fire with complex combination of longitudinal ventilation and ceiling extraction," *Applied Thermal Engineering*, vol. 110, p. 1021–1028, 2017.
- [14] X. Tian, M. Zhong, C. Shi, P. Zhang and C. Liu, "Full-scale tunnel fire experimental study of fire-induced smoke temperature profiles with methanol-gasoline blends," *Applied Thermal Engineering*, vol. 116, p. 233–243, 2017.
- [15] P. V. Ferkul and J. S. T'ien, "A Model of Low-Speed Concurrent Flow Flame Spread Over a Thin Fuel," *Combustion Science and Technology*, vol. 99, no. 4-6, pp. 345-370, 1994.
- [16] Y.-T. Tseng and J. S. T'ien, "Limiting Length, Steady Spread, and Nongrowing Flames in Concurrent Flow Over Solids," *Journal of Heat Transfer*, vol. 132, no. 9, p. 091201, 2010.
- [17] S. L. Olson and P. V. Ferkul, "Microgravity Flammability of PMMA Rods in Concurrent Flow," in *9th US National Combustion Meeting*, Cincinnati Ohio, 2015.
- [18] X. Zhao, Y.-T. T. Liao, M. C. Johnston, J. S. T'ien, P. V. Ferkul and S. L. Olson, "Concurrent flame growth, spread, and quenching over composite fabric samples in low speed purly forced flwo in microgravity," *Proceedings of the Combustion Institute*, vol. 36, pp. 2971-2978, 2017.

- [19] D. L. Urban, P. Ferkul, S. Olson, G. A. Ruff, J. Easton, J. S. T'ien, Y.-T. T. Liao, C. Li, C. Fernandez-Pello, J. L. Torero, G. Legros, C. Eigenbrod, N. Smirnov, O. Fujita, S. Rouvreau, B. Toth and G. Jomaas, "Flame spread: Effects of microgravity and scale," *Combustion and Flame*, vol. 199, pp. 168-182, 2019.
- [20] H.-Y. Shih and J. S. T'ien, "Modeling Wall Influence on Solid-Fuel Flame Spread in a Flow Tunnel," in *35th Aerospace Science Meeting & Exhibit*, Reno, NV, 1997.
- [21] S. L. Olson, P. V. Ferkul, S. Bhattacharjee, F. J. Miller, C. Fernandez-Pello, S. Link, J. S. T'ien and I. Wichman, "Results from on-board CSA-CP and CDM Sensor Readings during the Burning and Suppression of Solids II (BASS-II) Experiment in the Microgravity Science Glovebox (MSG)," in 45th International Conference on Environmental Systems, Bellevue, Washington, 2015.
- [22] S. Bhattacharjee, A. Simsek, O. Sandra and P. Ferkul, "The Critical Flow Velocity for Radiative Extinction in Opposed-Flow Flame Spread in a Microgravity Environment: A Comparison of Experimental, Computational, and Theoretical Results," *Combustion and Flame*, vol. 163, pp. 472-477, 2016.
- [23] X. Zhao, Y.-T. T. Liao, M. C. Johnston, J. S. T'ien, P. V. Ferkul and S. L. Olson, "Concurrent flame growth, spread, and quenching over composite fabric samples in low speed purely forced flow in microgravity," *Proceedings of the Combustion Institute*, vol. 36, no. 2, pp. 2971-2978, 2017.
- [24] X. Zhao and J. S. T'ien, "A three-dimensional transient model for flame growth and extinction in concurrent flows," *Combustion and Flame*, vol. 162, no. 5, pp. 1829-1839, 2015.
- [25] Y.-T. T. Liao and J. S. T'ien, "A numerical simulation of transient ignition and ignition limit of a composite solid by a localised radiant source," *Combustion Theory and Modelling*, vol. 17, no. 6, pp. 1096-1124, 2013.
- [26] D. Dietrich, H. Ross, Y. Shu, P. Chang and J. T'ien, "Candle Flames in Non-Buoyant Atmospheres," *Combustion science and technology*, vol. 156, pp. 1-24, 2000.
- [27] J. Buckmaster and Y. Zhang, "Oscillating edge-flames," Combustion Theory and Modelling, vol. 3, no. 3, pp. 547-565, 1999.
- [28] D. N. Schiller, H. D. Ross and W. A. Sirignano, "Computational Analysis of Flame Spread Across Alcohol Pools," *Combustion Science and Technology*, vol. 118, pp. 203-255, 1996.
- [29] K. M. N. Kumar and A. Kumar, "The Dynamics of Near Limit Self-propagating Flame over Thin Solid Fuels in Microgravity," *Proceedings of the Combustion Institute*, vol. 36, pp. 3081-3087, 2017.
- [30] S. L. Olson, F. J. Miller, S. Jahangirian and I. S. Wichman, "Flame Spread over Thin Fuels in Actual and Simulated

- Microgravity Conditions," *Combustion and Flame,* vol. 156, pp. 1214-1226, 2009.
- [31] S. Wang, S. Wang, K. Zhu, Y. Xiao and Z. Lu, "Near Quenching Limit Instabilities of Concurrent Flame Spread over Thin Solid Fuel," *Combustion Science and Technology*, vol. 188, no. 3, pp. 451-471, 2016.